



CHORUS

This is the accepted manuscript made available via CHORUS. The article has been published as:

Isotope-shift measurements and King-fit analysis in nickel isotopes

Kristian König, Felix Sommer, Jeremy Lantis, Kei Minamisono, Wilfried Nörtershäuser, Skyy Pineda, and Robert Powel

Phys. Rev. C **103**, 054305 — Published 11 May 2021

DOI: [10.1103/PhysRevC.103.054305](https://doi.org/10.1103/PhysRevC.103.054305)

Isotope-shift measurements and King-fit analysis in nickel

Kristian König,^{1,*} Felix Sommer,² Jeremy Lantis,¹ Kei Minamisono,¹
Wilfried Nörtershäuser,² Skyy Pineda,¹ and Robert Powel¹

¹*National Superconducting Cyclotron Laboratory, Michigan State University, East Lansing 48824, USA*

²*Institut für Kernphysik, Technische Universität Darmstadt, 64289 Darmstadt, Germany*

(Dated: March 29, 2021)

The isotope shifts of the $3d^9 4s \ ^3D_3 \rightarrow 3d^9 4p \ ^3P_2$ transition in the stable even-even nickel isotopes were measured. An improved accuracy was achieved by transforming the systematic contribution of the wavelength-meter-based laser-frequency measurement into a statistical-acting contribution by measuring the same observables at different frequency sets. A detailed King-fit analysis was performed to extract the mass-shift and field-shift parameters, which are crucial for the extraction of the charge radii of short-lived isotopes from recently measured isotope shifts. A critical dependence of the achievable charge-radius accuracy on the choice of the reference isotope in the King-fit analysis was observed and is discussed.

I. INTRODUCTION

Nickel isotopes at the proton shell closure of $Z = 28$ are of high interest to investigate a multitude of nuclear phenomena. For example, structural changes in the isotopic chain that includes the doubly magic ^{56}Ni and ^{78}Ni have been examined by measuring masses, lifetimes, spin, transition probabilities, excitation energies, electromagnetic moments and radii [1–4]. The existence of a subshell closure at $N = 40$ has been extensively discussed [5–8] as well as shape coexistence near ^{68}Ni and ^{78}Ni [9–12]. Collinear laser spectroscopy of isotopes in the nickel region can nuclear-model-independently access electromagnetic moments and nuclear charge radii and hence, enables a better understanding of the underlying physical phenomena [13–15].

Furthermore, precise nuclear-charge-radius measurements can be employed to constrain the neutron equation of state (EOS) [16–18]. Measurements of neutron-deficient nickel isotopes, e.g. ^{54}Ni , open the possibility to compare the charge radius to its isospin $T = 1$ mirror-pair partner (the stable ^{54}Fe) and to determine the neutron-skin thickness R_{skin} [19]. The neutron-skin thickness is proportional to $|N - Z| \cdot L$, with the neutron and proton number N and Z , respectively, and the coefficient L of the derivative of the symmetry energy at nuclear saturation density, which is important for the extrapolation of the EOS to lower and higher densities. Also, neutron-rich isotopes can be used to constrain L as demonstrated for ^{68}Ni [20]. There, R_{skin} was determined by combining a laser-spectroscopic charge-radius measurement with the dipole polarizability extracted from the pygmy and the giant dipole resonances [21].

Since collinear laser spectroscopy is the method of choice to deduce charge radii of short-lived isotopes from isotope-shift measurements, experiments in neutron-rich and neutron-deficient nickel isotopes have been performed at ISOLDE and NSCL, respectively, and are cur-

rently analyzed. Furthermore, measurements to extend these investigations to ^{52}Ni and ^{78}Ni are planned for the coming years. Since the $3d^9 4s \ ^3D_3 \rightarrow 3d^9 4p \ ^3P_2$ transition in neutral nickel is the best-suited optical transition for collinear laser spectroscopy [22], it is used for all measurements in radioactive nickel isotopes. To deduce the charge radii from the measured isotope shifts, a precise knowledge of atomic interactions, i.e. the mass-shift and field-shift parameters, is critical. The atomic parameters can be extracted in a King-fit analysis from isotope-shift measurements in stable isotopes with known radii [23]. Two precision measurements of the $3d^9 4s \ ^3D_3 \rightarrow 3d^9 4p \ ^3P_2$ transition were performed in stable nickel in the literature [20, 24]. They yield partly contradicting results, demanding a clarification to avoid systematic deviations in the evaluation of nuclear charge radii of radioactive isotopes.

In this paper, we present improved isotope-shift measurements in $^{58,60,62,64}\text{Ni}$ to resolve the discrepancy in the literature data. To increase the accuracy, a method to overcome systematic uncertainty limitations due to laser-frequency measurements with a wavelength meter was applied. This allows us to determine the mass-shift and field-shift parameters with higher precision. Our King-fit analysis is based on the improved procedure introduced by Hammen *et al.* [25] and we found a critical dependence between the choice of the reference isotope and the achievable charge-radius accuracy. These findings will enable a more precise determination of the charge radius of exotic nickel isotopes. The procedure and the corresponding uncertainty analysis are described in detail. It will be the basis for the analysis of the on-line measurements and can be easily applied for other isotopic chains.

II. SETUP

A schematic overview of the BEam COoling and LAsEr spectroscopy (BECOLA) facility at the NSCL/FRIB at Michigan State University is depicted in Fig.1 and a

* koenig@frib.msu.edu

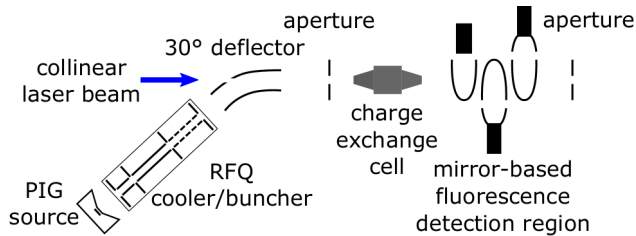


FIG. 1. Schematic of the BECOLA beamline. A Ni^+ ion beam was produced in a Penning-ionization-gauge (PIG) source. In the radio-frequency-quadrupole trap (RFQ) the beam was cooled and bunched. Laser and ion beams were superimposed and aligned through two 3-mm apertures at 2.1 m distance. The beam was neutralized through charge-exchange reactions with Na vapor. Fluorescence light was collected by three mirror-based detection units. Further ion optics for beam deflection and collimation are not shown.

detailed description can be found in [26, 27]. Singly-charged ion beams with a kinetic energy of 30 keV are available from either the NSCL/FRIB or from an off-line Penning-ionization-gauge (PIG) source [22]. The ions are guided into a helium-gas filled radio-frequency quadrupole trap (RFQ) [28], where they are cooled, accumulated and extracted as compressed ion bunches, which is a well-established technique for decreasing the constant laser-induced background [29, 30]. The ion beam is overlapped with a collinear laser beam in a 30° electrostatic deflector. The following 5-m long beamline includes several ion optical elements to ensure a good alignment of the beams, which can be checked by placing two 3-mm-diameter apertures at a distance of 2.1 m into the beamline. Between the apertures a sodium-loaded charge-exchange cell (CEC) [31] and three mirror-based fluorescence detection units (FDUs) are installed. The FDUs collect a large fraction of the fluorescence light and guide it to photo-multiplier tubes [26, 32]. The CEC and the FDUs can be floated on a scanning potential to perform Doppler tuning: Instead of scanning the laser frequency across the resonance, the beam velocity is adjusted by applying a small voltage that alters the beam energy, which results in different Doppler shifts. If the Doppler-shifted transition frequency matches the laser frequency, the ions or atoms emit fluorescence photons, which are counted with the photo-multiplier tubes.

In the present study, a Ni^+ ion beam was generated in the PIG off-line source from natural nickel. Since Ni^+ ions are not accessible by laser spectroscopy due to the lack of transitions in the optical regime, the ions had to be neutralized by collisions with Na vapor inside the charge-exchange cell. The CEC was heated to 410°C leading to a 50% neutralization efficiency of the incoming ion beam through electron donation from the Na vapor. Within this non-resonant process, various states were populated including the metastable $3d^9 4s^3 D_3$ state [22]. The atoms in this state were excited with laser light at 352 nm to the $3d^9 4p^3 P_2$ level.

The employed laser was a continuous-wave Ti-sapphire laser (Matisse 2 TS, Sirah Lasertechnik) that was operated at 704 nm and pumped by a frequency-doubled Nd-YAG solid state laser (Millennia eV, Spectra Physics). The 704-nm light was guided to a cavity-based frequency doubler (Wavetrain, Spectra Physics) creating the 352-nm light, which was transported via an optical fiber to the beamline and irradiated in collinear geometry. Spectroscopy was performed with a laser power of $300 \mu\text{W}$ and a laser-beam diameter of 1 mm at the interaction region. The short-term-frequency stabilization was realized by side-of-fringe locking to a reference cavity. For long-term stabilization, the cavity length was controlled by feedback from a wavelength meter (WSU30, HighFinesse), which continuously measured the laser frequency. The wavelength meter has a specified 3σ accuracy of 30 MHz for the absolute frequency reading. During the isotope shift measurements it was calibrated every minute to a helium-neon laser (SL 03, SIOS Metetechnik) that was frequency stabilized with the two-mode stabilization technique. Additionally, the wavelength meter was cross-referenced to an iodine-saturation-spectroscopy setup that was recently established at BECOLA. The setup is similar to those described in [33] and more details will be published elsewhere [34].

III. ISOTOPE SHIFTS OF STABLE NICKEL ISOTOPES

A. Measurement procedure

The isotope-shift measurements between the stable $^{58,60,62,64}\text{Ni}$ isotopes were performed by keeping the beam energy constant and changing the laser frequency for each isotope. Finally, Doppler tuning with a scanning range of 40 V was applied to determine the resonance position. Typical spectra are depicted in Fig. 2. Comparing the resonant rest-frame frequencies ν^A and $\nu^{A'}$ of one isotope and the reference isotope, respectively, yields the isotope-shift

$$\delta\nu^{A,A'} = \nu^A - \nu^{A'} . \quad (1)$$

Compared to the alternate approach, where the laser frequency is kept constant while the scan voltage is changed by a few kV when switching between the isotopes, the present procedure yields a smaller systematic uncertainty: The total beam energy can be determined precisely from a collinear and anticollinear measurement of one reference isotope and can be transferred to the other isotopes when performing all measurements at a constant acceleration voltage [36]. Contrarily, the electronic measurement of a large scanning voltage (2.7 kV to cover all isotopes for our conditions) can easily lead to uncertainties of a few MHz even if devices with 10^{-4} relative accuracy are applied. Furthermore, a change of the beam path was observed when changing the scanning potential. This was avoided in the present approach,

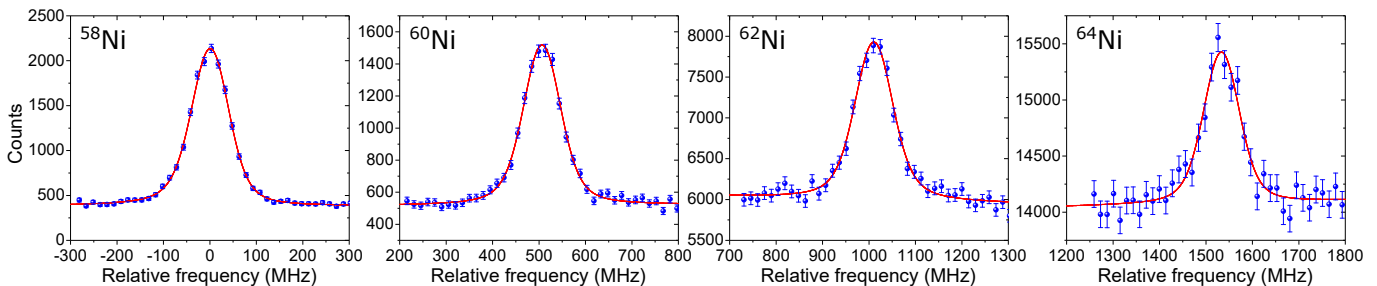


FIG. 2. Typical resonance spectra of $^{58,60,62,64}\text{Ni}$. Due to inelastic collisions during the charge exchange process [31], the lineshape is slightly asymmetric, which was considered in the fit function [35]. The abscissa is relative to ^{58}Ni .

where only small scanning voltages were applied. However, when changing the laser frequency, the uncertainty of the wavelength meter had to be considered. Recent studies on various devices of the same manufacturer as used here revealed that the offset of the wavelength meter reading from the real frequency is covered by the given specification. Local variations which are relevant for frequency differences within a scan region of a few GHz were about one order of magnitude smaller [37, 38]. In our case, the total uncertainty is specified to be ± 30 MHz (3σ) and the local variations were observed to be ± 3 MHz (3σ) for a similar device [38].

To determine and reduce the impact of these local variations, the isotope-shift measurements were performed with different laser-frequency sets, which became resonant at different beam energies. For each set, the laser frequencies were chosen in a way that all isotopes could be probed at the same beam energy. The measurements were repeated several times and at different days for each set. Within one frequency set, the obtained isotope shifts were consistent and the resulting statistical uncertainty was ≈ 0.6 MHz. Contrarily, when changing the beam energy to use a different frequency set, the results were systematically shifted as shown in Tab. I, where the beam-energy or frequency-set-dependent isotope shifts $\delta\nu^{60,58}$ are listed.

When considering the local variations of the wavelength meter, these results are in good agreement. From Gaussian error propagation of Eq. 1 an uncertainty of $2\sqrt{2}$ MHz (1σ) follows which includes a factor of two to account for the frequency doubling. Since the local variations of the wavelength-meter uncertainty are random for each frequency set [37, 38], this uncertainty contribution acts statistically when varying the resonant laser frequencies. Therefore, the respective $2\sqrt{2}$ -MHz contribution was added in quadrature to the fit uncertainties before calculating the weighted mean over the results obtained with different frequency sets. The final uncertainties following from Gaussian error propagation (1.1 MHz) and from the standard deviation of the mean (0.9 MHz) of the isotope shifts in Tab. I are consistent, which validates the error estimation concerning the wavelength meter. Conservatively, we take the larger value. Including additional systematic contributions (see section III C) leads

TABLE I. Isotope-shift measurements in the $3d^94s\ ^3D_3 \rightarrow 3d^94p\ ^3P_2$ transition between $^{60,58}\text{Ni}$ for different laser-frequency sets that were adjusted to match the Doppler-shifted transition frequencies at the listed beam energy. Typically, ten individual $^{60,58}\text{Ni}$ isotope-shift measurements were performed at each beam energy, yielding a fit uncertainty of ≈ 0.6 MHz. Local variations of the wavelength meter act statistically when using different laser-frequency sets (see text and Ref. [37, 38] for more details). Hence, the corresponding $2\sqrt{2}$ -MHz contribution was added to the fit uncertainty and the combined statistical uncertainty is given in squared brackets. It is used as weight for the evaluation of the weighted mean. From Gaussian error propagation follows a combined statistical uncertainty of 1.1 MHz. Further systematic contributions are added (see section III C) and the total uncertainty is listed in parentheses.

beam energy eV	$\delta\nu^{60,58}$ MHz
28475	504.3 [2.9]
28481	506.0 [2.8]
29100	504.1 [2.9]
29800	505.5 [2.9]
29909	510.9 [2.9]
30629	506.2 [2.9]
31552	506.7 [2.9]
Mean	506.3 [1.1] (2.3)

to a total uncertainty of 2.3 MHz for the isotope shift $\delta\nu^{60,58}$.

Alternative to average isotope shifts over the results taken with different frequency sets, the uncertainty of the frequency measurement can be reduced by employing more elaborate instruments, e.g., a frequency comb, or by using additional devices to measure the relative frequency in parallel like a scanning Fabry-Perot interferometer [37] or by referencing the laser frequency to a well-known natural transition line, e.g., from the I_2 spectrum. The latter technique has been recently established at BECOLA and was employed for a $^{60,58}\text{Ni}$ isotope-shift measurement. A pair of iodine lines was selected, for which both isotopes appeared at nearly the same beam energy. These iodine lines have been referenced against a frequency comb at TU Darmstadt and allowed us to re-

TABLE II. Results of $^{60,58}\text{Ni}$ isotope-shift measurements in the $3d^9 4s \ ^3D_3 \rightarrow 3d^9 4p \ ^3P_2$ transition based on three different approaches. In the first two cases, the wavelength-meter uncertainty was reduced by averaging over different frequency sets or by referencing it to well-known iodine lines. The same systematic contributions apply for these measurements (2.1 MHz, see section III C). Based on the independent uncertainties (fit and frequency determination, squared brackets), the weighted mean was taken and the common systematic contributions were added. The total uncertainty is given in parentheses. The isotope shift extracted from our collinear and anticollinear measurements [36] is regarded fully independent in terms of the systematic uncertainty. The weighted mean yields the final result. Literature values for the $^{60,58}\text{Ni}$ isotope shift are provided in Tab. III.

Method	$\delta\nu^{60,58}$ MHz
Wavelength meter	506.3 [1.1]
Iodine reference	507.0 [0.9]
Mean	506.7 [0.8] (2.2)
Col./Anticol. [36]	505.6 (3.9)
Final	506.4 (1.9)

duce the frequency-measurement uncertainty to 0.6 MHz [34]. The quadratic sum with the statistical uncertainty yielded 0.9 MHz. Otherwise, the same systematic uncertainties as in the normal wavelength-meter-referenced operation applied, which are discussed in section III C. The result is listed in Tab. II.

As a last method, the rest-frame frequencies of ^{58}Ni and ^{60}Ni from our collinear and anticollinear measurements [36] were used to extract the isotope shift between both isotopes. As shown in Tab. II, all three methods are in agreement. The final $\delta\nu^{60,58}$ isotope shift was calculated as the weighted mean of the three approaches. Since the same systematics apply for the first two methods, they were averaged in a first step, where only the independent uncertainties (fit and laser-frequency determination) were taken as weights, which are listed in squared brackets in Tab. II. Gaussian error propagation yielded 0.8 MHz. Adding the systematic uncertainty contributions (see section III C) leads to a total uncertainty of 2.2 MHz. This result was combined with the one obtained from collinear and anticollinear spectroscopy, yielding the final value of 506.4 (1.9) MHz.

All other isotope shifts presented in this paper were determined by applying only the first method that is based on averaging the results obtained with different frequency sets. The isotope shifts were measured at six different beam energies, each consisting of at least two independent data sets.

TABLE III. Isotope shifts in the $3d^9 4s \ ^3D_3 \rightarrow 3d^9 4p \ ^3P_2$ transition between the stable even-even nickel isotopes from the present work and the literature [20, 24]. Besides the measured results (m), Ref. [24] listed corrected values (c), which were improved by projecting the measurements on a King fit. All uncertainties are given for a 1σ interval.

	This work MHz	Ref. [20] MHz	Ref. [24] (m) MHz	Ref. [24] (c) MHz
$\delta\nu^{60,58}$	506.4 (1.9)	509.1 (4.9)	506.9 (1.0)	507.8 (0.9)
$\delta\nu^{62,58}$	1010.6 (2.4)	-	1021.7 (1.7)	1019.6 (1.5)
$\delta\nu^{64,58}$	1534.3 (2.6)	-	1533.1 (3.9)	1532.5 (3.1)
$\delta\nu^{62,60}$	504.4 (2.7)	503.9 (4.6)	507.2 (1.4)	506.9 (1.2)
$\delta\nu^{64,60}$	1028.2 (2.6)	1027.2 (8.1)	-	-
$\delta\nu^{64,62}$	524.7 (2.6)	-	503.1 (3.6)	509.9 (2.6)

B. Results

In Tab. III, the results of all investigated isotopes are listed and compared with the literature. Our isotope shifts are consistent with those from a collinear laser spectroscopy measurement performed at ISOLDE [20] and the deviations are much smaller than the denoted uncertainties. In the presented measurements the uncertainty was improved by a factor of two compared to Ref. [20].

The results also mostly agree with the measurements from a liquid-nitrogen-cooled hollow cathode [24] but particularly measurements including ^{62}Ni deviate in case of the investigated $3d^9 4s \ ^3D_3 \rightarrow 3d^9 4p \ ^3P_2$ transition. The results from Ref. [24] are published with a 3σ uncertainty which was reduced to 1σ for comparison. In their publication, they also list isotope shifts that are corrected by a King-fit analysis, which shifts their isotope shifts including ^{62}Ni closer to our values. Nevertheless, the data sets still deviate, which can be traced back to underestimated uncertainties in Ref. [24] by a detailed King-fit discussion in section IV C.

C. Uncertainty analysis

Due to the diverse natural abundance of the nickel isotopes $^{58,60,62,64}\text{Ni}$ (68.1% / 26.2% / 3.6% / 0.9%), the measurement time varied from < 5 min for $^{58,60}\text{Ni}$ to about one hour for ^{64}Ni . We did not investigate ^{61}Ni (1.1%) since hyperfine splitting leads to a further reduction of the signal strength. To compensate drifts of, e.g., the acceleration potential, the less-abundant isotopes were measured between the more abundant $^{58,60}\text{Ni}$ resulting in a $^{58}\text{Ni} - ^{60}\text{Ni} - ^{62}\text{Ni} - ^{64}\text{Ni} - ^{60}\text{Ni} - ^{58}\text{Ni}$ measurement scheme. When deriving the isotope shift relative to ^{58}Ni or ^{60}Ni , the respective isotope was used to calibrate the beam energy based on a collinear and anticollinear measurement [36]. Drifts of up to 0.3 eV were observed between the beginning and the end of the measurement cycle. The beam energy was linearly in-

terpolated and the time-corrected values were assigned to the $^{62,64}\text{Ni}$ measurements. $^{60,58}\text{Ni}$ isotope-shift measurements were not time corrected but only consecutive measurements were compared. These were mostly performed in alternating order ($^{58}\text{Ni} - ^{60}\text{Ni} - ^{60}\text{Ni} - ^{58}\text{Ni}$). In the data analysis, the photons that were counted by the three FDUs, were added before fitting and then the shift between two isotopes was extracted.

As discussed in section III A, the wavelength-meter uncertainty became statistical by performing measurements with different laser-frequency sets and hence, it was added in quadrature to the fit uncertainty before taking the weighted mean over the respective measurements. The resulting statistical uncertainties were between 1.1 and 1.7 MHz for the different isotope shifts. Additionally, the following systematic contributions were added in quadrature:

- *Beam energy determination:* < 0.3 MHz: As discussed in [36], the uncertainty of the beam-energy determination based on the collinear and anti-collinear approach is below 0.3 eV. For our experimental conditions, this results in small systematic uncertainties of $\Delta\delta\nu(\delta A = 2) = 0.07$ MHz, $\Delta\delta\nu(\delta A = 4) = 0.15$ MHz and $\Delta\delta\nu(\delta A = 6) = 0.22$ MHz, which depend on the mass difference δA .
- *Lineshape:* 0.5 MHz: An asymmetric lineshape is observed and expected due to inelastic collision during the charge exchange process [31]. Evaluating the data with a symmetric Voigt, a Voigt combined with a satellite at fixed frequency distance, and a Voigt with an exponential contribution [35], leads to deviations of the isotope shifts of up to 0.5 MHz. The latter function yielded the most consistent results in terms of reduced χ^2 , fluctuations of the results taken under the same conditions, and total uncertainty and was therefore chosen for the final results.
- *Bunching:* 2 MHz: The time gates for evaluating the bunched measurements were carefully chosen to collect 3σ of the bunch width. Varying the time-gate width and position leads to changes of a few 100 kHz. However, a systematically different isotope shift was observed when using a continuous beam instead of a bunched beam. The origin of this deviation is still unclear. Dependence on the gas pressure of the RFQ as well as on the amount of ions accumulated for bunching were investigated but neither resolved the difference. Testing this phenomenon in the $4s\ ^2\text{S}_{1/2} \rightarrow 4p\ ^2\text{P}_{3/2}$ transition of Ca^+ yielded consistent results with precision measurements in the literature [39, 40] in case of a bunched beam whereas the continuous-beam measurements showed a deviation. Conservatively, a 2-MHz contribution that bridges the gap outside the combined fit uncertainties was added to the presented results.

We neglected uncertainties due to an angular misalignment of the laser light and nickel atom beam since the applied beam-energy-determination method [36] yielded directly the velocity component in laser-beam direction. The ion and laser beam alignment was not changed during the measurements. Also, possible drifts of the helium-neon laser frequency that was used to calibrate the wavelength meter were neglected since the time interval between the reference measurements in $^{58,60}\text{Ni}$ was short.

IV. KING PLOT AND NUCLEAR CHARGE RADII

A. Method

As extensively discussed in the literature, the isotope shift $\delta\nu^{A,A'}$ originates from two effects: The mass shift, which arises from a displaced center of gravity and the respective nuclear motion with changing amount of neutrons, and the field shift that is caused by the different finite size of the nucleus

$$\delta\nu^{A,A'} = K\mu^{A,A'} + F\Lambda^{A,A'} \quad (2)$$

with the mass-shift constant K , the field-shift constant F , and the mass coefficient $\mu^{A,A'}$ [23]

$$\mu^{A,A'} = \frac{m_A - m_{A'}}{(m_A + m_e)(m_{A'} + m_e)} \quad (3)$$

where m_A and $m_{A'}$ are the nuclear masses, which we obtained from [41] and [42], and m_e is the electron mass. $\Lambda^{A,A'}$ is the nuclear parameter

$$\Lambda^{A,A'} = \delta\langle r^2 \rangle^{A,A'} + \frac{C_2}{C_1}\delta\langle r^4 \rangle^{A,A'} + \frac{C_3}{C_1}\delta\langle r^6 \rangle^{A,A'} + \dots \quad (4)$$

with the Seltzer coefficients C and the differential mean square charge radius $\delta\langle r^2 \rangle^{A,A'} = \langle r^2 \rangle^A - \langle r^2 \rangle^{A'}$ between the isotopes A and A' , etc. The higher-order contributions of the nuclear parameter consider that the electronic wave function is not constant across the nuclear volume, which is particularly important for heavy elements. For low and medium masses these contributions are small and $\Lambda^{A,A'} \approx \delta\langle r^2 \rangle^{A,A'}$. In the case of Ni, the approximation $\Lambda^{A,A'} \approx \delta\langle r^2 \rangle^{A,A'}$ causes a relative deviation of $< 0.05\%$ when extracting the differential mean square charge radius from a King plot, while the uncertainty of $\delta\langle r^2 \rangle^{A,A'}$ is $> 1\%$ for stable isotopes and even larger for rare isotopes.

For stable isotopes, precise literature values for the charge radii are available from muonic and electron-scattering experiments. These can be used in combination with isotope-shift measurements in a King-fit analysis [23]: Rearranging Eq.2 yields a linear relation between the modified isotope shifts $\delta\nu^{A,A'}/\mu^{A,A'}$ and the modified differential mean square charge radii

$$\delta\langle r^2 \rangle^{A,A'} / \mu^{A,A'}:$$

$$\frac{\delta V^{A,A'}}{\mu^{A,A'}} = F \frac{\delta\langle r^2 \rangle^{A,A'}}{\mu^{A,A'}} + K. \quad (5)$$

The field-shift and mass-shift parameters F and K , respectively, can be extracted experimentally if nuclear charge radii of at least three isotopes are available. These atomic factors are of utmost importance for extracting the charge radii of short-lived isotopes. Furthermore, the isotope-shift measurements can be validated by checking the quality of the expected linear relation. If isotope shifts of two or more transitions have been measured, the charge radius can be eliminated [23], enabling a validation based on the isotope shift measurements only and to determine the field-shift ratio [39, 40].

B. Treatment of reference charge radii

The established procedure for the extraction of the charge radii of stable reference isotopes is to combine tabulated muonic and electron-scattering data, e.g., Ref. [43]. In many of the published laser spectroscopic results, the reference table is quoted but the derivation of the not directly listed differential mean square charge radii $\delta\langle r^2 \rangle^{A,A'}$ and especially their uncertainty $\Delta\delta\langle r^2 \rangle^{A,A'}$ are often not specified. For this reason we want to provide a detailed description of the procedure applied here. We used the compilation from Fricke and Heilig [43] as is usually done in the laser spectroscopy community. They list the results from muonic experiments including the model-independent Barrett equivalent radii $R_{k\alpha}$. These can be combined with the also given electron-scattering results that reveal the ratio of radial moments V , yielding the model-independent charge radii

$$\langle r^n \rangle^{1/n} = R_{k\alpha} / V_n. \quad (6)$$

While the extraction of the differential mean square charge radius $\delta\langle r^2 \rangle^{A,A'}$ (and also of $\Lambda^{A,A'}$) is straightforward

$$\begin{aligned} \delta\langle r^2 \rangle^{A,A'} &= \langle r^2 \rangle^A - \langle r^2 \rangle^{A'} \\ &= \left(\frac{R_{k\alpha}^A}{V_2^A} \right)^2 - \left(\frac{R_{k\alpha}^{A'}}{V_2^{A'}} \right)^2 \\ &= \underbrace{\left(\frac{R_{k\alpha}^A}{V_2^A} - \frac{R_{k\alpha}^{A'}}{V_2^{A'}} \right)}_{\text{term I}} \cdot \underbrace{\left(\frac{R_{k\alpha}^A}{V_2^A} + \frac{R_{k\alpha}^{A'}}{V_2^{A'}} \right)}_{\text{term II}}, \end{aligned} \quad (7)$$

the determination of the corresponding uncertainty is often treated differently in the presentation of laser spectroscopic results. In some cases the full uncertainty of the Barrett radius is taken, in others the systematic contribution is (partly) neglected assuming it is canceled during the extraction of radii differences.

TABLE IV. Differential mean square charge radii extracted from Ref.[43] based on the relative Barrett radius from muonic measurements and the ratio of radial moments from elastic electron scattering experiments by the procedure described in the text.

Differential mean square charge radius	
fm ²	
$\delta\langle r^2 \rangle^{60,58}$	0.2731 (48)
$\delta\langle r^2 \rangle^{62,58}$	0.5000 (48)
$\delta\langle r^2 \rangle^{64,58}$	0.6362 (48)
$\delta\langle r^2 \rangle^{62,60}$	0.2266 (48)
$\delta\langle r^2 \rangle^{64,60}$	0.3631 (48)
$\delta\langle r^2 \rangle^{64,62}$	0.1365 (48)

In the table from Fricke and Heilig a detailed error estimation is given, which is adopted in the present work. They illustrate why the radial moments V should be treated without error and explain the uncertainties given for the Barrett radii: In the table, they provide an experimental Barrett-radius uncertainty, which combines the statistical and the energy-calibration contributions, and a theoretical Barrett-radius uncertainty originating from the calculation of the nuclear polarization correction. The latter is estimated to be less than 30% of the total nuclear polarization value. Furthermore, they point out that the uncertainty of relative Barrett-radii measurements is smaller. In that case the energy-calibration contribution cancels, which reduces the experimental uncertainty contribution, and they estimate the systematic uncertainty to be only 10% (30% for deformed nuclei) of the larger one of the nuclear polarization values of the two isotopes. For this reason, Fricke and Heilig also list values for the Barrett radii differences $\delta R_{k\alpha}^{AA'} = R_{k\alpha}^A - R_{k\alpha}^{A'}$ and the corresponding uncertainties $\Delta\delta R_{k\alpha}^{AA'}$. They generally list these only for neighboring isotopes but following their argumentation, this evaluation can be extended, i.e., to the difference between the Barrett radius of a common reference isotope and that of all other isotopes. We added the experimental and theoretical contributions in quadrature for the final value of $\Delta\delta R_{k\alpha}^{AA'}$.

To determine the uncertainty of the differential mean square charge radii by making use of the well-estimated uncertainties of the relative Barrett radii, term I in the rearranged Eq. 7 was approximated by $\delta R_{k\alpha}^{AA'} / V_2^{A'}$. This is justified for the uncertainty estimation since the ratio of radial moments V is treated without error and the relative difference of V_2^A and $V_2^{A'}$ is usually below one per mill. This then yields a simple equation for the uncertainty of the differential mean square charge radius:

$$\Delta\delta\langle r^2 \rangle \approx \frac{\Delta\delta R_{k\alpha}^{AA'}}{V_2^{A'}} \cdot \left(\frac{R_{k\alpha}^A}{V_2^A} + \frac{R_{k\alpha}^{A'}}{V_2^{A'}} \right). \quad (8)$$

The uncertainty contributions of $R_{k\alpha}^A$ and $R_{k\alpha}^{A'}$ in term II can be neglected since they are multiplied by the much smaller term I, which leads to a suppression by two orders of magnitude.

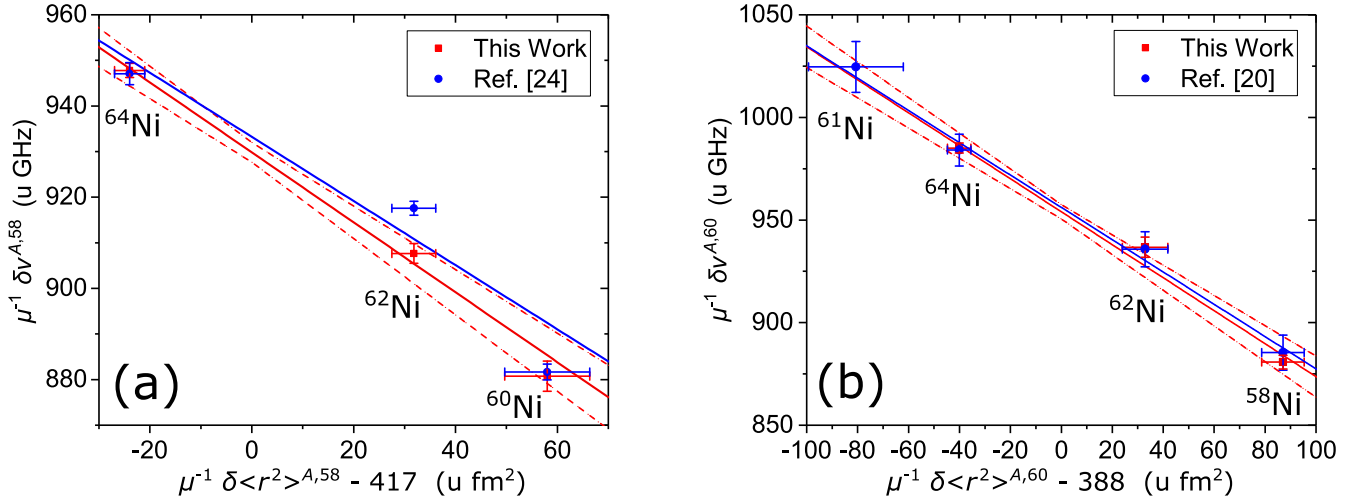


FIG. 3. King plots based on (a) the isotope shifts $\delta\nu^{A,58}$ of the present work (red) and of Ref. [24] (blue), (b) the isotope shifts $\delta\nu^{A,60}$ of the present work (red) and of Ref. [20] (blue), and the differential mean square charge radii of Tab. IV. The straight solid red line was obtained by the linear regression applied to our data (blue for literature data) and the dashed lines show the 1σ confidence interval. The dominant contribution to the fit uncertainty is the uncertainty of the modified differential mean squared charge radii.

The differential mean square charge radii of $^{58,60,62,64}\text{Ni}$ with the corresponding uncertainties that were extracted by the described procedure are listed in Tab. IV.

C. King-fit analysis

For performing a King-fit analysis of the isotope shifts presented in Tab. III, the procedure introduced by Hammen *et al.* [25] was applied that shifts the origin of the abscissa by introducing a constant offset parameter α

$$\frac{\delta\nu^{A,A'}}{\mu^{A,A'}} = F \left(\frac{\delta\langle r^2 \rangle^{A,A'}}{\mu^{A,A'}} - \alpha \right) + K_\alpha \quad (9)$$

to reduce the correlation between the atomic parameters K and F . The impact of α on K and F becomes small close to the minimal correlation and, hence, we limited α in the optimization procedure to integer numbers. The linear regression was performed according to the method of York *et al.* [44]. King fits with ^{58}Ni and ^{60}Ni as reference isotope are depicted in Fig. 3.

Charge radii can then be extracted from the isotope-shift measurements with the obtained atomic factors as

$$\delta\langle r^2 \rangle^{A,A'} = \frac{\delta\nu^{A,A'} - \mu^{A,A'} K_\alpha}{F} + \mu^{A,A'} \alpha. \quad (10)$$

Compared to the standard procedure, the uncorrelated atomic factors allow for a determination of the corresponding uncertainty simply by Gaussian error propaga-

tion since the correlation matrix is diagonal

$$\Delta\delta\langle r^2 \rangle^{A,A'} = \left[\left(\frac{\Delta\delta\nu^{A,A'}}{F} \right)^2 + \left(\frac{\mu^{A,A'}}{F} \Delta K_\alpha \right)^2 + \left(\left(\alpha - \frac{K_\alpha}{F} \right) \Delta\mu^{A,A'} \right)^2 + \left(\frac{\delta\nu^{A,A'} - \mu^{A,A'} K_\alpha \Delta F}{F^2} \right)^2 \right]^{\frac{1}{2}}. \quad (11)$$

Since the mass-shift constant K becomes dependent on the free parameter α , it loses its physical meaning. For this reason, both results for the mass-shift parameter are listed in Tab. V: K_α where α was optimized to reduce the correlation, and K_0 , where $\alpha = 0$. The King-fit analysis was performed in three different ways: First, the most abundant isotope ^{58}Ni was used as global reference A' , second, ^{60}Ni was employed as global reference isotope as done in Ref. [20], and third, a King fit was performed in ladder style, which means that isotope shifts and mean-square charge radii differences of neighboring isotopes were used with $A > A'$.

Comparing F and K_0 of the three different approaches yields a good agreement. Furthermore, all of our values agree well with the atomic factors given in Ref. [20], where ^{60}Ni was used as global reference isotope. This is also illustrated by the King plots (Fig. 3b). It should be noted that $\delta\nu^{61,60}$ was additionally measured in Ref. [20], which gave further weight in their King fit. When using the isotope shifts between $^{60,62,64}\text{Ni}$ and ^{58}Ni from Ref. [24] (see Tab. III) to perform a King-fit analysis, it yields smaller values for K_0 and F , which agree, however, still within the uncertainty interval. Analyzing the corresponding King plot (Fig. 3a) with ^{58}Ni as global reference isotope shows that our mass-modified isotope-shifts

TABLE V. Results from King-fit analyses based on our $3d^9 4s\ 3D_3 \rightarrow 3d^9 4p\ 3P_2$ isotope-shift measurements $\delta\nu^{A,A'}$ (see Tab. III) and the differential mean square charge radii extracted from Ref. [43] by the procedure described in the text (see Tab. IV). King fits with ^{58}Ni and ^{60}Ni as global reference A' and in ladder style were performed. The extracted atomic factors are compared to those published in Ref. [20]. We also performed a King-fit analysis with the isotope shifts from Ref. [24]. The field-shift parameter F (in MHz/fm²) and the independent mass-shift parameter K_0 (in GHz/u) are in agreement within the different analyses. Furthermore, K_α (in GHz/u) is given where an offset parameter α (in u fm²) was optimized to reduce the correlation between K_α and F . Due to the dependence on α , the values of K_α cannot be directly compared.

	$\delta\nu^{A,58}$	$\delta\nu^{A,60}$	$\delta\nu^{\text{ladder}}$	$\delta\nu^{A,60}$ [20]	$\delta\nu^{A,58}$ [24]
F	-767 (70)	-804 (66)	-765 (57)	-788 (82)	-702 (67)
K_0	1250 (29)	1266 (26)	1249 (24)	1262 (32)	1227 (29)
K_α	929.8 (2.2)	954.0 (3.5)	938.3 (4.7)	949 (4)	927.0 (2.2)
α	417	388	406	397	426

align with the mass-modified mean square charge radii. Contrarily, the isotope shifts from Ref. [24] show some disagreement, which indicates that the uncertainties of isotope-shift measurements from Ref. [24] might be underestimated.

D. Choice of the reference isotope

When analyzing the uncertainties of K_α and F of the three different choices of the reference isotope in more detail, it is noted that $\Delta K_\alpha(^{58}\text{Ni}) < \Delta K_\alpha(^{60}\text{Ni}) < \Delta K_\alpha(\text{ladder})$ while $\Delta F(^{58}\text{Ni}) > \Delta F(^{60}\text{Ni}) > \Delta F(\text{ladder})$. In ladder style, the largest range in the King-plot diagram is covered, leading to smaller uncertainties of the slope (F) but to larger uncertainties of the intercept (K_α) compared to the case with ^{58}Ni as global reference, where the data is compressed into the smallest range (see Fig. 3). Even though these differences seem marginal, they are significant in the charge-radii evaluation of short-lived isotopes.

We want to demonstrate the importance of the choice of the reference isotope for the example of ^{54}Ni . The achievable accuracy of the differential mean square charge radius $\Delta\delta\langle r^2 \rangle^{54,A'}$ is plotted in Fig. 4 for the atomic factors that were extracted with ^{58}Ni and ^{60}Ni as global reference isotope, in dependence of the yet unknown isotope shift $\delta\nu^{54,58}$, which is expected to be between -1.3 and -1.5 GHz. The minima in these curves are defined by the first two terms in Eq. 11 (neglecting the usually much smaller mass term) and, hence, depend on ΔK_α and on the isotope-shift uncertainty $\Delta\delta\nu^{54,A'}$. To differentiate between both contributions, the resulting uncertainty is plotted for an isotope shift uncertainty of 0 MHz (solid line) and 10 MHz (dashed line). Due to the smaller mass coefficient $\mu^{A,A'}$ and since

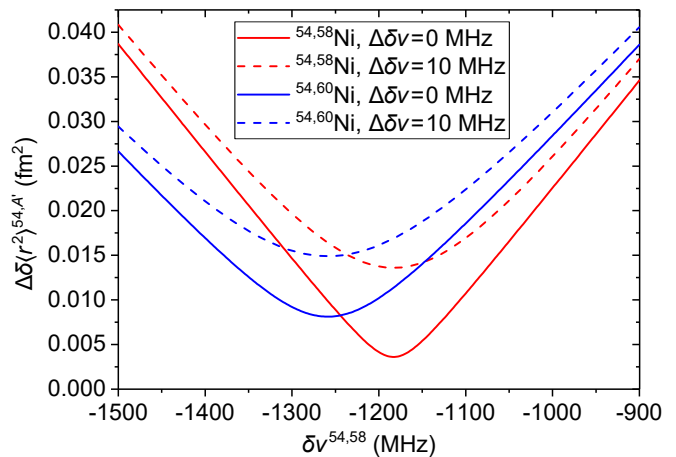


FIG. 4. Uncertainty of the differential mean square charge radius $\Delta\delta\langle r^2 \rangle^{54,A'}$ extracted from an isotope-shift measurement $\delta\nu^{54,A'}$. The reference isotope dependence originates in the different uncertainties of K_α and F and the distance to the reference isotopes in the King-plot diagram. The minimum is located at the center of the reference isotopes. To disentangle the impact of the uncertainties of atomic factors and isotope-shift measurement, the resulting uncertainty is plotted for $\Delta\delta\nu^{54,A'} = 0$ MHz and $\Delta\delta\nu^{54,A'} = 10$ MHz. See text for more details.

$\Delta K_\alpha(^{58}\text{Ni}) < \Delta K_\alpha(^{60}\text{Ni})$, a lower minimum is reached in case of ^{58}Ni as reference. Contrarily, the slope of the achievable accuracy depends on the last term in Eq. 11 that describes the ΔF contribution and hence, favors ^{60}Ni as reference isotope. The minima are shifted relative to each other since they depend on where $\delta\nu^{54,A'}$ is located in the respective King plot: The highest accuracy is reached if the isotope of interest is located in the center of the King plot, which varies for the different reference isotopes.

For an isotope shift of $\delta\nu^{54,58} < -1.25$ GHz, a smaller uncertainty of the differential mean square charge radius is reached by choosing ^{60}Ni as reference isotope instead of the more abundant ^{58}Ni . For example, assuming an isotope shift of $\delta\nu^{54,58} = -1.4$ GHz and an experimental uncertainty of 10 MHz, the resulting uncertainty of the differential mean square charge radius would be 30 % smaller. Therefore, the charge-radius accuracy can be significantly improved by a wise choice of the reference isotope, which is particularly important if absolute radii are of interest, e.g., for constraining the equation of state of nuclear matter [19].

V. CONCLUSION

An approach to overcome the limitations of a conventional wavelength meter was presented. Local variations in its response that were revealed recently in detailed investigations on these devices [37, 38] can strongly affect the achievable accuracy of relative frequency mea-

measurements. By varying the laser frequency sets, the uncertainty of the wavelength meter acts statistically and, hence, is reduced with an increasing number of independent measurements. Applying this method, the accuracy of the isotope shifts of the $3d^9 4s \ ^3D_3 \rightarrow 3d^9 4p \ ^3P_2$ transition in the stable $^{58,60,62,64}\text{Ni}$ isotopes was improved by a factor of two compared to previous laser spectroscopic investigations [20]. A King-fit analysis confirms the robustness of our data and reveals underestimated uncertainties in Ref. [24], whose isotope shifts partly deviate from our values, whereas the results of Ref. [20] are in agreement with our measurements. This resolves the discrepancy between both literature measurements and allows for a more reliable charge-radius extraction of short-lived nickel isotopes.

Furthermore, three different King-fit analyses were evaluated, in which the isotope-shift measurements refer either to ^{58}Ni , ^{60}Ni or the neighbouring isotope. These methods span different ranges in the King-plot diagram,

leading to different uncertainties in the extraction of slope and offset of a fitted line. A critical dependence of the achievable accuracy of the differential mean square charge radii from the chosen reference isotope was found and illustrated for the example of ^{54}Ni . This approach can be easily applied for other isotopic chains and will be a useful technique to improve the accuracy of further charge-radius measurements.

VI. ACKNOWLEDGEMENTS

We thank Phillip Ingram and Julian Palmes (both TU Darmstadt) for referencing the iodine lines to the frequency comb. This work was supported in part by the National Science Foundation under Grant No. PHY-15-65546. F.S. acknowledges funding by the Deutsche Forschungsgemeinschaft (DFG, German Research Foundation) Project-ID 279384907 SFB 1245.

-
- [1] C. Guénaut, G. Audi, D. Beck, K. Blaum, G. Bollen, P. Delahaye, F. Herfurth, A. Kellerbauer, H.-J. Kluge, J. Libert, D. Lunney, S. Schwarz, L. Schweikhard, and C. Yazidjian, *Phys. Rev. C* **75**, 044303 (2007).
- [2] J. S. Berryman, K. Minamisono, W. F. Rogers, B. A. Brown, H. L. Crawford, G. F. Grinyer, P. F. Mantica, J. B. Stoker, and I. S. Towner, *Phys. Rev. C* **79**, 064305 (2009).
- [3] Z. Y. Xu, S. Nishimura, G. Lorusso, F. Browne, P. Doornenbal, G. Gey, H.-S. Jung, Z. Li, M. Niikura, P.-A. Söderström, T. Sumikama, J. Taprogge, Z. Vajta, H. Watanabe, J. Wu, A. Yagi, K. Yoshinaga, H. Baba, S. Franchoo, T. Isobe, P. R. John, I. Kojouharov, S. Kubono, N. Kurz, I. Matea, K. Matsui, D. Mengoni, P. Morfouace, D. R. Napoli, F. Naqvi, H. Nishibata, A. Odahara, E. Şahin, H. Sakurai, H. Schaffner, I. G. Stefan, D. Suzuki, R. Taniuchi, and V. Werner, *Phys. Rev. Lett.* **113**, 032505 (2014).
- [4] R. Taniuchi, C. Santamaria, P. Doornenbal, A. Obertelli, K.-i. Yoneda, G. Authelet, H. Baba, D. Calvet, F. Chteau, A. Corsi, A. Delbart, J. Gheller, A. Gillibert, J. Holt, T. Isobe, V. Lapoux, M. Matsushita, J. Menendez, S. Momiyama, and Z. Xu, *Nature* (2019).
- [5] R. Broda, B. Fornal, W. Królas, T. Pawlat, D. Bazzacco, S. Lunardi, C. Rossi-Alvarez, R. Menegazzo, G. de Angelis, P. Bednarczyk, J. Rico, D. De Acuña, P. J. Daly, R. H. Mayer, M. Sferrazza, H. Grawe, K. H. Maier, and R. Schubart, *Phys. Rev. Lett.* **74**, 868 (1995).
- [6] O. Sorlin, S. Leenhardt, C. Donzaud, J. Duprat, F. Azaiez, F. Nowacki, H. Grawe, Z. Dombrádi, F. Amorini, A. Astier, D. Baiborodin, M. Bellegruic, C. Borcea, C. Bourgeois, D. M. Cullen, Z. Dlouhy, E. Dragulescu, M. Górska, S. Grévy, D. Guillemaud-Mueller, G. Hagemann, B. Herskind, J. Kiener, R. Lemmon, M. Lewitowicz, S. M. Lukyanov, P. Mayet, F. de Oliveira Santos, D. Pantalica, Y.-E. Penionzhkevich, F. Pougheon, A. Poves, N. Redon, M. G. Saint-Laurent, J. A. Scarpaci, G. Sletten, M. Stanoiu, O. Tarasov, and C. Theisen, *Phys. Rev. Lett.* **88**, 092501 (2002).
- [7] K. Langanke, J. Terasaki, F. Nowacki, D. J. Dean, and W. Nazarewicz, *Phys. Rev. C* **67**, 044314 (2003).
- [8] D. Pauwels, J. L. Wood, K. Heyde, M. Huyse, R. Julin, and P. Van Duppen, *Phys. Rev. C* **82**, 027304 (2010).
- [9] S. Suchyta, S. N. Liddick, Y. Tsunoda, T. Otsuka, M. B. Bennett, A. Chemey, M. Honma, N. Larson, C. J. Prokop, S. J. Quinn, N. Shimizu, A. Simon, A. Spyrou, V. Tripathi, Y. Utsuno, and J. M. VonMoss, *Phys. Rev. C* **89**, 021301 (2014).
- [10] B. Crider, C. Prokop, S. Liddick, M. Al-Shudifat, A. Ayangeakaa, M. Carpenter, J. Carroll, J. Chen, C. Chiara, H. David, A. Dombos, S. Go, R. Grzywacz, J. Harker, R. Janssens, N. Larson, T. Lauritsen, R. Lewis, S. Quinn, F. Recchia, A. Spyrou, S. Suchyta, W. Walters, and S. Zhu, *Phys. Lett. B* **763**, 108 (2016).
- [11] F. Nowacki, A. Poves, E. Caurier, and B. Bounthong, *Phys. Rev. Lett.* **117**, 272501 (2016).
- [12] A. Gade and S. N. Liddick, *J. Phys. G Nucl. Partic.* **43**, 024001 (2016).
- [13] M. L. Bissell, T. Carette, K. T. Flanagan, P. Vingerhoets, J. Billowes, K. Blaum, B. Cheal, S. Fritzsche, M. Godefroid, M. Kowalska, J. Krämer, R. Neugart, G. Neyens, W. Nörtershäuser, and D. T. Yordanov, *Phys. Rev. C* **93**, 064318 (2016).
- [14] X. F. Yang, C. Wraith, L. Xie, C. Babcock, J. Billowes, M. L. Bissell, K. Blaum, B. Cheal, K. T. Flanagan, R. F. Garcia Ruiz, W. Gins, C. Gorges, L. K. Grob, H. Heylen, S. Kaufmann, M. Kowalska, J. Kraemer, S. Malbrunot-Ettenauer, R. Neugart, G. Neyens, W. Nörtershäuser, J. Papuga, R. Sánchez, and D. T. Yordanov, *Phys. Rev. Lett.* **116**, 182502 (2016).
- [15] R. P. de Groote, J. Billowes, C. L. Binnersey, M. L. Bissell, T. E. Cocolios, T. Day Goodacre, G. J. Farooq-Smith, D. V. Fedorov, K. T. Flanagan, S. Franchoo, R. F. Garcia Ruiz, A. Koszorús, K. M. Lynch, G. Neyens, F. Nowacki, T. Otsuka, S. Rothe, H. H. Stroke, Y. Tsunoda, A. R. Vernon, K. D. A. Wendt, S. G. Wilkins, Z. Y. Xu, and X. F. Yang, *Phys. Rev. C* **96**, 041302 (2017).

- [16] M. B. Tsang, J. R. Stone, F. Camera, P. Danielewicz, S. Gandolfi, K. Hebeler, C. J. Horowitz, J. Lee, W. G. Lynch, Z. Kohley, R. Lemmon, P. Möller, T. Murakami, S. Riordan, X. Roca-Maza, F. Sammarruca, A. W. Steiner, I. Vidaña, and S. J. Yennello, *Phys. Rev. C* **86**, 015803 (2012).
- [17] B. A. Brown, *Phys. Rev. Lett.* **119**, 122502 (2017).
- [18] J. Yang and J. Piekarewicz, *Phys. Rev. C* **97**, 014314 (2018).
- [19] B. A. Brown, K. Minamisono, J. Piekarewicz, H. Hergert, D. Garand, A. Klose, K. König, J. D. Lantis, Y. Liu, B. Maaß, A. J. Miller, W. Nörtershäuser, S. V. Pineda, R. C. Powel, D. M. Rossi, F. Sommer, C. Sumithrarachchi, A. Teigelhöfer, J. Watkins, and R. Wirth, *Phys. Rev. Res.* **2**, 022035 (2020).
- [20] S. Kaufmann, J. Simonis, S. Bacca, J. Billowes, M. L. Bissell, K. Blaum, B. Cheal, R. F. G. Ruiz, W. Gins, C. Gorges, G. Hagen, H. Heylen, A. Kanellakopoulos, S. Malbrunot-Ettenauer, M. Miorelli, R. Neugart, G. Neyens, W. Nörtershäuser, R. Sánchez, S. Sailer, A. Schwenk, T. Ratajczyk, L. V. Rodríguez, L. Wehner, C. Wraith, L. Xie, Z. Y. Xu, X. F. Yang, and D. T. Yordanov, *Phys. Rev. Lett.* **124**, 132502 (2020).
- [21] D. M. Rossi, P. Adrich, F. Aksouh, H. Alvarez-Pol, T. Aumann, J. Benlliure, M. Böhmer, K. Boretzky, E. Casarejos, M. Chartier, A. Chatillon, D. Cortina-Gil, U. Datta Pramanik, H. Emling, O. Ershova, B. Fernandez-Dominguez, H. Geissel, M. Gorska, M. Heil, H. T. Johansson, A. Junghans, A. Kelic-Heil, O. Kiselev, A. Klimkiewicz, J. V. Kratz, R. Krücken, N. Kurz, M. Labiche, T. Le Bleis, R. Lemmon, Y. A. Litvinov, K. Mahata, P. Maierbeck, A. Movsesyan, T. Nilsson, C. Nociforo, R. Palit, S. Paschalis, R. Plag, R. Reifarth, D. Savran, H. Scheit, H. Simon, K. Sümmerner, A. Wagner, W. Waluś, H. Weick, and M. Winkler, *Phys. Rev. Lett.* **111**, 242503 (2013).
- [22] C. Ryder, K. Minamisono, H. Asberry, B. Isherwood, P. Mantica, A. Miller, D. Rossi, and R. Strum, *Spectrochim. Acta B* **113**, 16 (2015).
- [23] W. H. King, *Isotope Shifts in Atomic Spectra* (Springer Science+Business Media, New York, 1984).
- [24] A. Steudel, U. Triebe, and D. Wendlandt, *Z. Phys. A* **296**, 189 (1980).
- [25] M. Hammen, W. Nörtershäuser, D. L. Balabanski, M. L. Bissell, K. Blaum, I. Budinčević, B. Cheal, K. T. Flanagan, N. Frömmgen, G. Georgiev, C. Geppert, M. Kowalska, K. Kreim, A. Krieger, W. Nazarewicz, R. Neugart, G. Neyens, J. Papuga, P.-G. Reinhard, M. M. Rajabali, S. Schmidt, and D. T. Yordanov, *Phys. Rev. Lett.* **121**, 102501 (2018).
- [26] K. Minamisono, P. Mantica, A. Klose, S. Vinnikova, A. Schneider, B. Johnson, and B. Barquest, *Nucl. Instrum. Methods Phys. Res., A* **709**, 85 (2013).
- [27] D. M. Rossi, K. Minamisono, B. R. Barquest, G. Bollen, K. Cooper, M. Davis, K. Hammerton, M. Hughes, P. F. Mantica, D. J. Morrissey, R. Ringle, J. A. Rodriguez, C. A. Ryder, S. Schwarz, R. Strum, C. Sumithrarachchi, D. Tarazona, and S. Zhao, *Rev. Sci. Instrum.* **85**, 093503 (2014).
- [28] B. Barquest, G. Bollen, P. Mantica, K. Minamisono, R. Ringle, S. Schwarz, and C. Sumithrarachchi, *Nucl. Instrum. Methods Phys. Res., A* **866**, 18 (2017).
- [29] A. Nieminen, P. Campbell, J. Billowes, D. H. Forrest, J. A. R. Griffith, J. Huikari, A. Jokinen, I. D. Moore, R. Moore, G. Tungate, and J. Äystö, *Phys. Rev. Lett.* **88**, 094801 (2002).
- [30] P. Campbell, H. L. Thayer, J. Billowes, P. Dendooven, K. T. Flanagan, D. H. Forest, J. A. R. Griffith, J. Huikari, A. Jokinen, R. Moore, A. Nieminen, G. Tungate, S. Zemlyanoi, and J. Äystö, *Phys. Rev. Lett.* **89**, 082501 (2002).
- [31] A. Klose, K. Minamisono, C. Geppert, N. Frömmgen, M. Hammen, J. Krämer, A. Krieger, C. Levy, P. Mantica, W. Nörtershäuser, and S. Vinnikova, *Nucl. Instrum. Methods Phys. Res., A* **678**, 114 (2012).
- [32] B. Maaß, K. König, J. Krämer, A. Miller, K. Minamisono, W. Nörtershäuser, and F. Sommer, “A 4π Fluorescence Detection Region for Collinear Laser Spectroscopy,” (2020), arXiv:2007.02658 [physics.ins-det].
- [33] S. Reinhardt, B. Bernhardt, C. Geppert, R. Holzwarth, G. Huber, S. Karpuk, N. Miskioğlu, W. Nörtershäuser, C. Novotny, and T. Udem, *Opt. Commun.* **274**, 354 (2007).
- [34] R. Powel, M. Koble, J. Palmes, N. Everett, P. Imgram, K. König, J. Lantis, K. Minamisono, W. Nörtershäuser, R. Parker, S. Pineda, F. Sommer, and A. Klose, “Calibration of laser frequency for collinear laser spectroscopy via doppler-free spectroscopy of molecular iodine,” in preparation (2021).
- [35] A. L. Stancik and E. B. Brauns, *Vib. Spectrosc.* **47**, 66 (2008).
- [36] K. König, K. Minamisono, J. Lantis, S. Pineda, and R. Powel, *Phys. Rev. A* **103**, 032806 (2021).
- [37] M. Verlinde, K. Dockx, S. Geldhof, K. König, D. Studer, T. Cocolios, R. de Groote, R. Ferrer, Y. Kudryavtsev, T. Kieck, I. Moore, W. Nörtershäuser, S. Raeder, P. Bergh, P. Van Duppen, and K. Wendt, *Appl. Phys. B* **126**, 85 (2020).
- [38] K. König, P. Imgram, J. Krämer, B. Maa, K. Mohr, T. Ratajczyk, F. Sommer, and W. Nörtershäuser, *Appl. Phys. B* **126**, 86 (2020).
- [39] C. Shi, F. Gebert, C. Gorges, S. Kaufmann, W. Nörtershäuser, B. Sahoo, A. Surzhykov, V. Yerokhin, J. Berengut, F. Wolf, J. Heip, and P. Schmidt, *Appl. Phys. B* **123**, 2 (2016).
- [40] P. Müller, K. König, P. Imgram, J. Krämer, and W. Nörtershäuser, *Phys. Rev. Res.* **2**, 043351 (2020).
- [41] M. Wang, G. Audi, F. G. Kondev, W. Huang, S. Naimi, and X. Xu, *Chinese Phys. C* **41**, 030003 (2017).
- [42] NIST, “Atomic Spectra Database Ionization Energies Form,” (2021).
- [43] G. Fricke and K. Heilig, *Nuclear Charge Radii* (Springer, Berlin Heidelberg, 2004).
- [44] D. York, N. M. Evensen, M. L. Martinez, and J. De Basabe Delgado, *Am. J. Phys.* **72**, 367 (2004).